Observation of the Protonated Semiquinone Intermediate in Isolated Reaction Centers from *Rhodobacter sphaeroides*: Implications for the Mechanism of Electron and Proton Transfer in Proteins†

M. S. Graige, M. L. Paddock, G. Feher, and M. Y. Okamura*

Department of Physics, 0319, University of California, San Diego, La Jolla, California 92093-0319 U.S.A.

Received March 26, 1999

ABSTRACT: A proton-activated electron transfer (PAET) mechanism, involving a protonated semiquinone intermediate state, had been proposed for the electron-transfer reaction $k_{AB}^{(2)}$ [$Q_A^{-\bullet}Q_B^{-\bullet} + H^+ \rightleftarrows Q_A^{-\bullet}(Q_BH)^\bullet \rightarrow Q_A(Q_BH)^-$] in reaction centers (RCs) from *Rhodobacter sphaeroides* [Graige, M. S., Paddock, M. L., Bruce, M. L., Feher, G., and Okamura, M. Y. (1996) *J. Am. Chem. Soc. 118*, 9005−9016]. Confirmation of this mechanism by observing the protonated semiquinone $(Q_BH)^\bullet$ had not been possible, presumably because of its low pK_a. By replacing the native Q_{10} in the Q_B site with rhodoquinone (RQ), which has a higher pK_a, we were able to observe the $(Q_BH)^\bullet$ state. The pH dependence of the semiquinone optical spectrum gave a pK_a = 7.3 ± 0.2. At pH < pK_a, the observed rate for the $k_{AB}^{(2)}$ reaction was constant and attributed to the intrinsic electron-transfer rate from $Q_A^{-\bullet}$ to the protonated semiquinone (i.e., $k_{AB}^{(2)} = k_{ET}(RQ) = 2 \times 10^4\ s^{-1}$). The rate decreased at pH > pK_a as predicted by the PAET mechanism in which fast reversible proton transfer precedes rate-limiting electron transfer. Consequently, near pH 7, the proton-transfer rate $k_H \gg 10^4\ s^{-1}$. Applying the two step mechanism to RCs containing native Q_{10} and taking into account the change in redox potential, we find reasonable values for the fraction of $(Q_BH)^\bullet \cong 0.1\%$ (consistent with a p$K_a(Q_{10})$ of ∼4.5) and $k_{ET}(Q_{10}) \cong 10^6\ s^{-1}$. These results confirm the PAET mechanism in RCs with RQ and give strong support that this mechanism is active in RCs with Q_{10} as well.

Electron and proton transfers are coupled in many biological reactions that involve energy conversion (*1*). In photosynthetic bacteria, the reaction center (RC)[1] protein catalyzes the conversion of electromagnetic energy to chemical energy through the two-electron, two-proton reduction of a bound secondary quinone, Q_B (*2*, *3*):

$$Q_B + 2\,e^- + 2\,H^+ \xrightarrow{2h\nu} Q_BH_2 \qquad (1)$$

A crucial intermediate step in eq 1 is the transfer of the second electron that is coupled to proton transfer. This reaction has been postulated to proceed via a two-step process involving the intermediate protonated state, $Q_BH^\bullet$, as described by eq 2 (*4*).

$$Q_A^-{}^\bullet\, Q_B^-{}^\bullet + H^+ \underset{}{\overset{k_{H^+}}{\rightleftharpoons}} Q_A^-{}^\bullet\,(\mathbf{Q_BH})^\bullet \xrightarrow{k_{ET}} Q_A(Q_BH)^- \qquad (2)$$
$$\xrightarrow{\qquad\qquad k_{AB}^{(2)} \qquad\qquad}$$

For this mechanism, protonation of $Q_B^{-\bullet}$ precedes rate-limiting electron transfer from $Q_A^{-\bullet}$. *The protonated semiquinone intermediate, $Q_BH^\bullet$, had so far not been observed in isolated RCs*. The goal of this work was to observe the intermediate state, which would provide compelling evidence for the validity of eq 2. In particular, the presence of an intermediate would eliminate the mechanism involving a concerted proton/electron transfer (*4*−*7*). In addition, observation of the protonated intermediate state would enable one to measure k_{ET} and to establish a limit for k_{H^+}.

The reason that the protonated intermediate had not been observed previously is because ubisemiquinone in isolated native RCs ($Q_{10(B)}^{-\bullet}$) has a low pK value, which results in a small steady-state concentration of $Q_BH^\bullet$. A straightforward solution to this problem was to synthesize a quinone with a higher pK value. This was accomplished by replacing one of the methoxy substituents of Q_{10} by an amine group creating a rhodoquinone (RQ) (Figure 1) that could be incorporated into the Q_B site of the RC. Unfortunately, concomitant with the increase in the pK value, the redox potential of RQ was reduced by ∼80 mV (*8*). This makes the transfer of the first electron from $Q_A^{-\bullet}Q_B$ to $Q_AQ_B^{-\bullet}$ thermodynamically unfavorable. To overcome this problem, we incorporated a low potential naphthoquinone (NQ) into the Q_A binding site.

The experiments reported in this work were performed on RCs having RQ in the Q_B binding site. A comparison between the known $QH^\bullet$ optical absorbance spectrum in solution and the semiquinone spectrum measured in these RCs gave strong evidence of $Q_BH^\bullet$ formation. The pH dependencies of the semiquinone optical spectrum and the

* To whom correspondence should be addressed. Telephone: (619) 543-2506. Fax: 619-822-0007. E-mail: mokamura@ucsd.edu.

† Supported by NIH 2 RO1GM 41637, NIH GM 13191, and NSF MCB 94-16652.

[1] Abbreviations: RC, reaction center; PAET, Proton-Activated Electron Transfer; D, primary donor; Q_A, primary acceptor; Q_B, secondary acceptor; Q_{10}, coenzyme Q_{10}; RQ, rhodoquinone; NQ, naphthoquinone; MQ_4, menatetrenone; Me_3NQ, 2,3,5-trimethyl-1,4-naphthoquinone; Me_4NQ, 2,3,6,7-tetramethyl-1,4-naphthoquinone; RQ_B-RC, RC with RQ in the Q_B binding site.

10.1021/bi990708u CCC: $18.00
Published on Web 08/12/1999

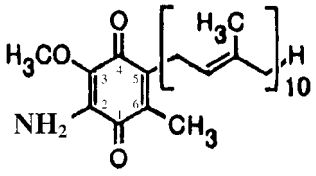

FIGURE 1: The structures of rhodoquinone (RQ). For Q_{10}, the NH_2 at position 2 is a methoxy group. This substitution has the effect of lowering the redox potential and raising the p*K* of RQ relative to Q_{10} (*8*).

transfer rate of the second electron, $k_{AB}^{(2)}$ were measured. From these measurements not only the mechanism of proton coupled electron transfer but also the intrinsic electron-transfer k_{ET} and a lower limit for k_{H^+} were determined for this system. The results are strictly valid only for RCs having RQ_B. However, in view of the similarity between RQ and Q_{10}, we believe that the conclusions of this work are applicable to native RCs. A preliminary account of this work has been published (*9*).

MATERIALS AND METHODS

Quinones. Q_{10} (coenzyme Q_{10}, 2,3-dimethoxy-5-methyl-6-decaisoprenyl-1,4-benzoquinone) and MQ_4 (menatetrenone; 2-methyl-3-tetraisoprenyl-1,4-naphthoquinone) were obtained from Sigma. Me_3NQ (2,3,5-trimethyl-1,4-naphthoquinone) and Me_4NQ (2,3,6,7-tetramethyl-1,4-naphthoquinone) were kindly provided by J. M. Bruce, University of Manchester, UK. RQ (rhodoquinone; 2-amino-3-methoxy-6-methyl-5-decaisoprenyl-1,4-benzoquinone) was obtained by two methods. (1) Biosynthetically: *Rhodospirillum rubrum* was grown photosynthetically under anaerobic conditions (*10*). Quinone was isolated from the cells using a method described previously for quinone extraction (*11, 12*). The biosynthetically produced RQ was separated from Q_{10} using TLC as described in the second method. (2) Synthetically: RQ was obtained by a one-step conversion of Q_{10} to RQ (*13*). Separation from the Q_{10} starting material and side products, which included iso-RQ (2-amino-3-methoxy-5-methyl-6-decaisoprenyl-1,4-benzoquinone), was performed as described (*13, 14*) using preparative TLC plates (Whatman, PK6F and PE SilG). Identity and purity of RQ (>98%) and iso-RQ (>98%) were confirmed by NMR and optical spectroscopy. After recrystalization, the final yield of RQ was ~1%; the melting point was 69 °C. Synthetic RQ had identical functional properties and optical spectra as RQ produced biosynthetically. All quinones were solubilized in ethanol prior to use. Q_{10} and RQ were also solubilized in 1% LDAO.

Reagents and Buffers. Ferrocene (fe, Eastman Kodak) and diaminodurene (DAD: 2,3,5,6-tetramethyl-1,4-phenylenediamine, Aldrich) were solubilized in ethanol and used to reduce the photooxidized primary donor, D^+. Terbutryne (Chem Service) and stigmatellin (Fluka) were also prepared in ethanol. Unless otherwise indicated, experiments were performed at 23 °C in BMK-buffer that consisted of 0.04% maltoside (dodecyl-β-D-maltoside, Anatrace) 10 mM KCl (Fisher) and 5 mM of each of the following buffers: citric acid (Calbiochem), mes (2-N-morpholinoethanesulfonic acid, Calbiochem), pipes (1,4-piperazine bis ethanesulfonic acid, Calbiochem), tris (2-amino-2-(hydroxymethyl)propane-1,3-diol, Fisher), ches (cyclohexylaminoethanesulfonic acid, Calbiochem), and caps (3-cyclohexylamino-1-propanesulfonic acid, Calbiochem). All reagents were of analytical grade.

The pH of the solution was adjusted by adding either 1M caps buffer (pH 10.5) or 1M citrate buffer (pH 4.5). pH measurements were performed with a Cole-Palmer Chemcadet pH meter equipped with an Toledo-Mettler U402-M3 pH electrode and calibrated with standards that spanned the measured pH values. The uncertainty in reported pH values was ± 0.05 units.

Sample Preparation. RCs from *Rb. sphaeroides* strain R26.1 were isolated in LDAO (lauryldimethylamine N oxide, Fluka) as described previously (*15*). Both Q_A and Q_B were removed as described (*16, 17*) by washing RCs on a DEAE column (Toyopearl 650M, Supelco) with 4% LDAO, 20 mM 1,10-phenanthroline (Fisher) and 1 mM 2-mercaptoethanol (Fluka) to yield RCs with ≤2% residual Q_A/RC and ≤0.2% residual Q_B/RC (as determined from the charge recombination rate and amplitude measured at 865 nm (*18*)). The ratio of absorbance, A^{280}/A^{800}, was 1.20. RCs were concentrated to ~0.1 mM by centrifugation (Amicon Centricon-30) and dialyzed for 20 h at 4 °C against BMK buffer, pH 7.2.

A detailed procedure for reconstitution of the Q_A binding site with naphthoquinone (NQ) has been presented previously (*4*). Briefly, quinone-depleted RCs in buffer were added to a reaction vial that contained a dried film of NQ. The quantity of NQ added was determined by its solubility in the buffer and the amount that was expected to be bound to the RC. The RCs were incubated in the reaction vial (30 °C, ~30 min with stirring) to yield RCs having full Q_A site occupancy and activity. The procedure to reconstitute the Q_A site with RQ was identical to the standard procedure for reconstitution with Q_{10}; it involved addition of the quinone solubilized in 1% LDAO to quinone-depleted RCs. This procedure resulted in full Q_A site occupancy by RQ.

After Q_A reconstitution, the Q_B site was reconstituted either by incubation with RQ adsorbed to Celite (diatomaceous earth, Fisher) for ~20 min at 25 °C, while stirring (*4*) or by addition of RQ (3 RQ: 1 RC) solubilized in 1% LDAO. Occupancy of the Q_B sites varied from 76 to 93% over the range of pH studied. The binding of NQ to the Q_A site is stronger than that of RQ; the binding of RQ to the Q_B site is stronger than that of NQ. This favorable situation resulted in ≥90% of the RCs with an occupied Q_B site, having a NQ in the Q_A site and RQ in the Q_B site.

Kinetic Measurements. Absorbance changes were measured using a single beam spectrophotometer of local design (*19*). The voltage output was recorded on a digital oscilloscope (Lecroy 9310M) and transferred to a PC for analysis. Fits to the data were made using nonlinear curve fitting software (Peakfit, TableCurve 2D or Sigmaplot, Jandel). Actinic illumination was provided by a pulsed dye laser (Phase R DL2100c, 590 nm, ~0.2J/pulse, 0.4-μs fwhm) and by a ruby laser (Optic Technologies Model 130, 695 nm, ~0.5 J/pulse, ~10ns fwhm). Laser light intensity was determined to be saturating (>98%) before and after each set of experiments. Scattered laser light was blocked from reaching the PMT by using a grating monochromator (Bausch and Lomb, 33-86-02) and cutoff filters.

Optical Spectrum of $Q_A^{-\bullet}$. The *in situ* optical absorbance spectra for $NQ_A^{-\bullet}$ and $RQ_A^{-\bullet}$ were obtained by measuring the optical change due to a saturating laser flash in RCs having only Q_A, i.e. ($DQ_A + fe_{red} \xrightarrow{h\nu} DQ_A^{-\bullet} + fe_{ox}$) where fe_{red} and fe_{ox} are the reduced and oxidized forms of ferrocene,

the exogenous electron donor. Ferrocene was chosen as the reductant for D^+ because of its negligible absorption in the wavelength region from 400 to 500 nm.

Optical Spectrum of $Q_B^{-\bullet}$ and $(Q_BH)^\bullet$. The in situ optical spectrum of rhodosemiquinone in the Q_B site was obtained using the procedure outlined above with corrections for: (*i*) the occupancy of the Q_B site, i.e. the fraction, δ, of RCs that lack Q_B, and (*ii*) the partition coefficient for the thermodynamic equilibrium, $[Q_A^{-\bullet}Q_B \rightleftarrows Q_AQ_B^{-\bullet}]$, α (*19*). Thus, at high pH where the unprotonated intermediate state dominates, the reaction equation is: $DQ_AQ_B + fe_{red} \xrightarrow{h\nu} (1-\alpha)(1-\delta)DQ_AQ_B^{-\bullet} + \alpha(1-\delta)DQ_A^{-\bullet}Q_B + \delta DQ_A^{-\bullet} + fe_{ox}$. A similar expression applies at low pH where the protonated intermediate state dominates and the first term on the right-hand side involves the protonated state $Q_AQ_BH^\bullet$.

Charge Recombination. The charge recombination rate, k_{AD} ($D^+Q_A^{-\bullet} \rightarrow DQ_A$), was determined by monitoring the recovery of the primary donor (D) absorbance at 865 nm following a saturating laser flash in RCs containing only Q_A. The charge recombination rate, k_{BD} ($D^+Q_AQ_B^{-\bullet} \rightarrow DQ_AQ_B$), was obtained by monitoring the slow phase of the primary donor recovery after a laser flash in RCs with both Q_A and Q_B binding sites occupied (*18*). The occupancy of the Q_B site and the thermodynamic equilibrium, $Q_A^{-\bullet}Q_B \rightleftarrows Q_AQ_B^{-\bullet}$, were determined from the kinetics of charge recombination (*18*, *19*).

Rate of the First Electron Transfer, $k_{AB}^{(1)}$. The electron-transfer rate $k_{AB}^{(1)}$ ($Q_A^{-\bullet}Q_B \rightarrow Q_AQ_B^{-\bullet}$) was measured in RQ_B-RCs by monitoring the absorption change at 420 nm following a saturating laser flash (*20*).

Rate of the Second Electron Transfer, $k_{AB}^{(2)}$. The rate of the second electron transfer, $k_{AB}^{(2)}$, was determined by monitoring the decay of semiquinone absorbance at 420 nm following a second laser flash in RC solutions containing the exogenous reductant, ferrocene, which reduces D^+ with a characteristic time of 5 ms (*21*). To ensure that the transients associated with the reduction of D^+ did not interfere with the measurements of $k_{AB}^{(2)}$, the observed rates were also measured with DAD ($\sim$100 μM) as the exogenous reductant (characteristic time of D^+ reduction is $\sim$30 ms). Terbutryne and stigmatellin block electron transfer to Q_B (*22*, *23*). Consequently, comparison of the flash induced kinetics before and after the addition of these inhibitors allowed the identification of the kinetics associated with Q_B reduction.

EXPERIMENTAL RESULTS AND ANALYSES

Characterization of the $(NQ_A)(RQ_B)$-RCs. Quinone-depleted RCs were incubated with NQ and the absorbance changes at 865 nm following a saturating laser flash were measured. From the kinetics of the charge recombination, $D^+Q_A^{-\bullet} \rightarrow DQ_A$ ($k_{AD} = 21\ s^{-1}$), and the amplitude of the absorbance change, we determined that the Q_A site was nearly fully occupied ($\geq$96%). Subsequent incubation of the RCs in the presence of RQ produced a slow phase in the charge recombination kinetics, characteristic of the Q_B site being occupied by RQ ($\geq$76%). Oscillations in absorbance at 420 nm were characteristic of the two-electron gate function of Q_B (*24*, *25*) and confirmed the incorporation of RQ into the Q_B site. Addition of terbutryne, which blocks electron transfer to Q_B, restored the charge recombination kinetics observed before RQ incubation showing that RQ did not displace NQ from the Q_A site. From the results of these experiments we concluded that $\geq$90% of RCs that had an occupied Q_B site had the $(NQ_A)(RQ_B)$ construct. We shall call these RCs, henceforth, RQ_B-RCs.

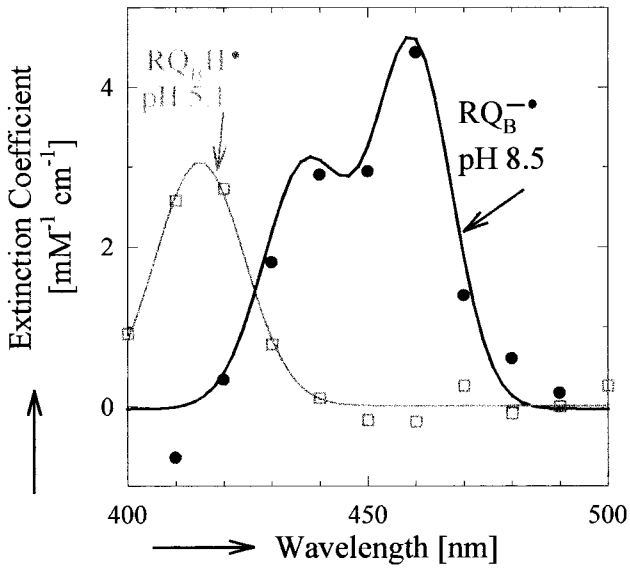

FIGURE 2: Optical spectra for rhodosemiquinone in the Q_B site. The spectra at high and low pH strongly resemble the anionic and protonated spectra of semiquinones in solution (*26*). Spectra were obtained from the absorbance changes at descrete wavelengths following a single saturating laser flash in the presence of the exogenous reductant, ferrocene. The spectrum for rhodosemiquinone in the Q_A site was, within experimental error, the same as the high pH spectrum shown. The solid lines show a smooth fit to the data generated using a single Gaussian function (low pH) and a sum of two Gaussians (high pH). Conditions: 6 μM RQ_B-RCs ($Me_4NQ_{(A)}$; $RQ_{(B)}$), 30 μM ferrocene, spectral bandwidth = 10 nm.

pH Dependence of the Optical Spectra of Rhodosemiquinone. Optical absorbance spectra of rhodosemiquinone in RQ_B-RCs (i.e., $RQ_B^{-\bullet}$ or $RQ_BH^\bullet$) were measured after a single saturating laser flash at several pH values. The spectrum determined at pH 5.1 was characteristic of protonated semiquinone ($\epsilon_{Max}^{420nm} = 3.0 \pm 0.2\ mM^{-1}\ cm^{-1}$), whereas the spectrum at pH 8.5 was characteristic of anionic semiquinone ($\epsilon_{Max}^{450nm} = 6.0 \pm 0.7\ mM^{-1}\ cm^{-1}$) (*26*) (see Figure 2). The spectrum at pH 8.5 was within experimental error the same as that for $RQ_A^{-\bullet}$, that is, the same as for rhodosemiquinone in the proton inaccessible Q_A site. This suggested that at pH 8.5, $RQ_B^{-\bullet}$ is fully ionized.

The fraction of RQ_B-RCs with rhodosemiquinone protonated, $f(RQ_BH^\bullet)$, was determined by fitting the observed spectra at intermediate pH values with a superposition of protonated and ionized rhodosemiquinone reference spectra. The spectra used as references were the $RQ_BH^\bullet$ spectrum determined in the Q_B site at pH = 5.1 and the $RQ^{-\bullet}$ spectrum determined in the Q_A site. The calculated $f(RQ_BH^\bullet)$ as a function of pH is shown in Figure 3. A fit to the data, given by the Henderson−Hasselbalch equation

$$f(RQ_BH^\bullet) = 1/[1+10^{pH-pK}] \qquad (3)$$

with pK = 7.3, is shown in Figure 3.[2]

In contrast to the results for RQ_B-RCs, the semiquinone spectra for RCs with native Q_{10} in the Q_B site resembled the anionic spectrum over the pH range from 4 to 9 (data not shown).

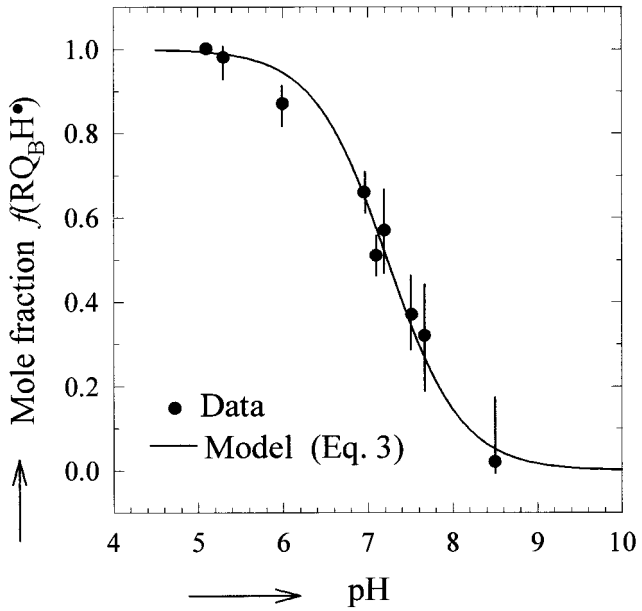

FIGURE 3: The fraction of protonated semiquinone, $f(RQ_BH^\bullet)$, as a function of pH. The fraction was determined by a simultaneous least-squares fit of the rhodosemiquinone absorbance spectra at intermediate pH values to the function: $A(\lambda_i)_{pH} = f(RQ_BH^\bullet) \times A(\lambda_i)_{RQ_BH^\bullet} + [1 - f(RQ_BH^\bullet)] \times A(\lambda_i)R_{Q_B}{}^{-\bullet}$ over the range of wavelength from 400 nm $= \lambda_i = 500$ nm. Error bars represent the uncertainty in the fitted value of $f(RQ_BH^\bullet)$ and include the uncertainties associated with the $RQ_BH^\bullet$ and $RQ_B{}^{-\bullet}$ reference spectra. The fitted curve (solid line) represents classical titration behavior (eq 3) with p$K = 7.3$. Conditions as given in Figure 2.

pH Dependence of Charge Recombination, k_{AD}. Calculation of the energy gap between the states, $Q_A{}^{-\bullet}Q_B$ and $Q_AQ_B{}^{-\bullet}$, important in later sections for estimating the driving force for electron transfer between the quinones, requires a knowledge of the charge recombination rates k_{AD} ($D^+Q_A{}^{-\bullet} \rightarrow DQ_A$) *and* k_{BD} ($D^+Q_AQ_B{}^{-\bullet} \rightarrow DQ_AQ_B$). The pH dependence of k_{AD} for RCs with Me_4NQ in the Q_A site is shown in Figure 4a. k_{AD} for RCs with other $NQ_{(A)}$ have been presented previously (*4, 17, 35, 36*).

The charge recombination rate k_{AD} for RCs with RQ in the Q_A site was measured in RCs with only one quinone (RQ_A). We expect the rate to vary with the free energy gap between the $D^+Q_A{}^{-\bullet}$ and DQ_A states and, therefore, it should be sensitive to the redox potential of Q_A (*35*). Surprisingly, the rate for RQ shown in Figure 4a is similar to that for Q_{10} ($\sim 8\ s^{-1}$) suggesting little change in the in situ redox potential despite the estimated difference of ~ 80 mV in redox potential between RQ and Q_{10} in solution. Possible explanations for this observation include: (*i*) a change in the reorganization energy that compensates for the change in redox potential and/or (*ii*) a difference in the hydrogen bond strength or solvation between RQ and Q_{10}.

pH Dependence of Charge Recombination, k_{BD}. The pH dependence of k_{BD} in RQ_B-RCs is shown in Figure 4b. The measured rates vary from 0.5 to 14 s^{-1} with the slope of the dependence gradually decreasing toward higher pH. At high pH, k_{BD} approaches the value of k_{AD}, which makes a reliable determination of k_{BD} difficult.

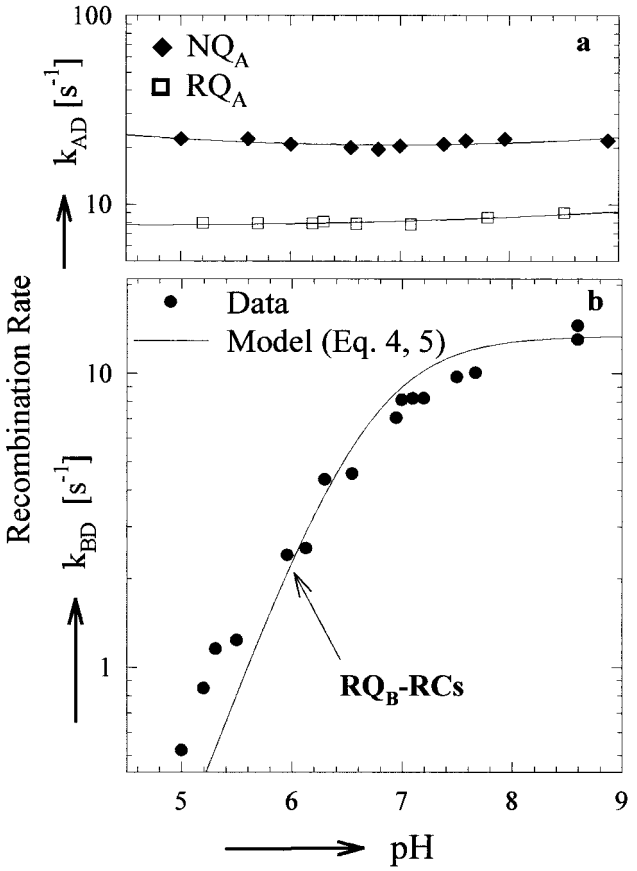

FIGURE 4: pH dependence of the charge recombination reactions, measured at 865 nm by monitoring the recovery of the primary donor (D) absorption after a laser flash. (a) Charge recombination, k_{AD}, $[D^+(Me_4NQ_A{}^{-\bullet}) \rightarrow D(Me_4NQ_A)]$ ◆, and $[D^+(RQ_A{}^{-\bullet}) \rightarrow D(RQ_A)]$ □. Solid lines show a smooth fit to the data. The statistical uncertainty in k_{AD} was $\leq$ 2% (b) Charge recombination, k_{BD}, $[D^+(Me_4NQ_A)(RQ_B{}^{-\bullet}) \rightarrow D(Me_4NQ_A)(RQ_B)]$. Solid line represents the fit to eq 5 with $pK_{(RQ_BH.)} = 7.0$. The statistical uncertainty in k_{BD} was $\leq$3%. Conditions: 1 μM one-quinone RCs for (a) and 1−6 μM RQ_B-RCs ($Me_4NQ_{(A)}$; $RQ_{(B)}$) for (b).

The model used to describe the k_{BD} recombination reaction involves the states, $D^+Q_A{}^{-\bullet}Q_B$, $D^+Q_AQ_B{}^{-\bullet}$, and $D^+Q_A(Q_BH)^\bullet$ as shown in eq 4.

$$DQ_AQ_B \underset{k_{AD}}{\overset{h\nu}{\rightleftharpoons}} D^+Q_A{}^{-\bullet}Q_B \underset{k_{BA}}{\overset{k_{AB}}{\rightleftharpoons}} D^+Q_AQ_B{}^{-\bullet} \underset{k_{H^+}^{off}}{\overset{k_{H^+}^{on}}{\rightleftharpoons}} D^+Q_A(Q_BH)^\bullet \quad (4)$$

Charge recombination proceeds indirectly through the thermally populated state, $D^+Q_A{}^{-\bullet}Q_B$, as has been shown for native RCs (*19*). In the model of eq 4, an equilibrium between the charge separated states is maintained ($k_{H^+}^{on}$, $k_{H^+}^{off}$, k_{AB} and $k_{BA} \gg k_{AD}$) and the observed rate can be written

$$k_{BD}^{obs.} = k_{AD}\, f(D^+Q_A{}^{-\bullet}Q_B) = k_{AD} \frac{1}{1 + \exp[-\Delta G_{AB}/k_BT](1 + 10^{pK-pH})} \quad (5)$$

where $f(D^+Q_A{}^{-\bullet}Q_B)$ is the equilibrium population of the $D^+Q_A{}^{-\bullet}Q_B$ state, ΔG_{AB} is the free energy between the

[2] In general, the electrostatic interactions between titrating sites within a protein give rise to complex titration behavior (*27, 28*). We neglect for simplicity interactions of the semiquinone with titratable amino acids in the protein. Deviation from classical behavior can be modeled using proton uptake data (*29*−*33*) and assuming a mean-field approximation (*34*). The mean field approach also gives a good fit to the data.

$D^+Q_A^{-\bullet}Q_B$ and $D^+Q_AQ_B^{-\bullet}$ states and pK refers to protonation of $Q_B^{-\bullet}$. The experimental data were fitted to eq 5 with pK as an adjustable parameter. ΔG_{AB} is essentially pH independent and was determined at pH 8.6 to have a value of 7 ± 5 meV; at this pH, the $D^+Q_A(Q_BH)^\bullet$ state population is negligible and $\Delta G_{AB} = -k_BT \ln[(k_{AD} - k_{BD})/k_{BD}]$ (*19*). The fit of eq 5 with pK = 7.0 to the experimental data is shown in Figure 4b.[2]

pH Dependence of $k_{AB}^{(1)}$ in RQ_B-RCs. The electron-transfer rate $k_{AB}^{(1)}$ ($Q_A^{-\bullet}Q_B \rightarrow Q_AQ_B^{-\bullet}$) was measured in RQ_B-RCs by monitoring the absorption change at 420 nm following a saturating laser flash (20). The kinetics of RQ_B-RCs over the pH range from 5 to 8.6 were, within experimental error, identical to those of native RCs. Since the $k_{AB}^{(1)}$ reaction is rate limited by protein dynamics and/or Q_B movement (*20*, *37*−*39*), these results indicate that substitution by RQ_B does not affect the dynamics and supports the assumption that RQ interacts with the RC in a manner similar to native Q_{10}. This is not surprising since the quinones interact with the protein via the carbonyl oxygens, which are structurally the same for both quinones.

pH dependence of $k_{AB}^{(2)}$ in RQ_B-RCs. The rate constant, $k_{AB}^{(2)}$ (eq 2), was obtained from the optical absorbance changes at 420 nm, measured for RQ_B-RCs in the presence of an exogenous donor after two laser flashes. The absorbance changes were biphasic at all pH. The faster phase (τ = 3 μs) was assigned to the decay of the triplet state ($DQ_A^{-\bullet} + h\nu \rightarrow D^TQ_A^{-\bullet} \xrightarrow{3\mu s} DQ_A^{-\bullet}$). This assignment was based on the known rate and spectrum (*40*), the insensitivity to terbutryne, and the correlation with the fraction of RCs having $Q_A^{-\bullet}$. Although at high pH the amplitudes of the two phases became comparable, the rate for each phase could be determined accurately because of the large difference in time scale.

The slower phase was terbutryne sensitive and was assigned to the transfer of the second electron, $NQ_A^{-\bullet}(RQ_BH^\bullet) \rightarrow NQ_A(RQ_BH)^-$, i.e. $k_{AB}^{(2)}$ (see Figure 5). This assignment was corroborated by correlating the wavelength dependence of the amplitude of the kinetic changes with the steady-state semiquinone spectra (data not shown). The slow phase could be well-fitted with a single exponential at all pH.

The pH dependence of $k_{AB}^{(2)}$ in RQ_B-RCs is shown in Figure 6. The rate is roughly pH independent at low pH and decreases at high pH by approximately a factor of 10 per pH unit. This dependence can be well-fitted, as described below, using the previously proposed proton-activated electron transfer (PAET) mechanism (eq 2) (*4*).

In this PAET mechanism, fast-reversible proton transfer occurs prior to rate-limiting electron transfer. The rate will be a function of the fraction of protonated intermediate state, $f(Q_BH^\bullet)$, and the forward electron-transfer rate, k_{ET}

$$k_{AB}^{(2)} = f(Q_BH^\bullet)\, k_{ET} \qquad (6)$$

where the fraction, $f(Q_BH^\bullet)$ is given by $f(Q_BH^\bullet) = 1/[1 + \exp -(\Delta G_{H^+}^0 / k_BT)] = 1/[1+10^{pH-pK}]$, $\Delta G_{H^+}^0$ is the free energy for protonation of $Q_B^{-\bullet}$ and pK is the pK of $Q_BH^\bullet$. Neglecting semiquinone−protein interactions, $f(Q_BH^\bullet)$ is expected to be approximately 1 for pH ≪ pK and decrease by a factor of 10 per pH unit for pH ≫ pK. The electron-transfer rate, k_{ET}, depends on free energy as given by the Marcus theory (*41*). Based on proton uptake measurements (*29*−*33*) the electron-transfer free energy changes by less than 10 meV per pH unit over the range of pH studied; thus, k_{ET} is expected to remain nearly constant with pH. The experimental data were fitted using eq 6 with $k_{ET} = 2 \times 10^4$ s^{-1} and pK as an adjustable parameter. The fit to the data with pK = 8.0 is shown in Figure 6.[2]

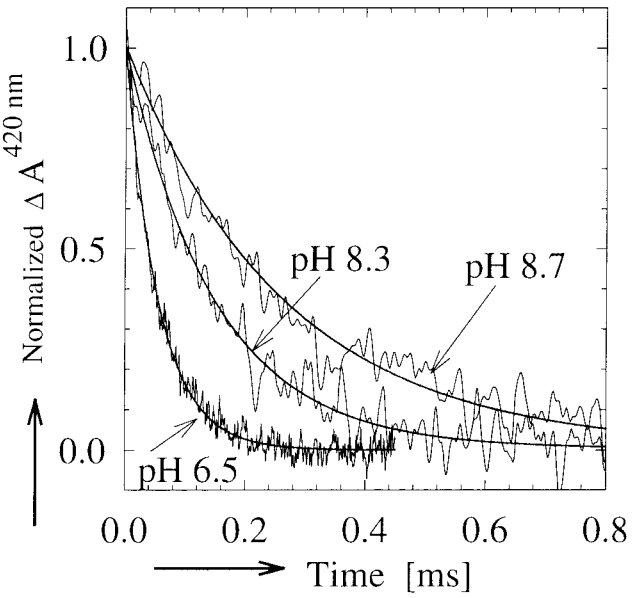

FIGURE 5: Optical absorbance changes associated with the transfer of the second electron in the reaction $k_{AB}^{(2)}$, $[NQ_A^{-\bullet}][RQ_B^{-\bullet}(H)] \rightarrow [NQ_A][RQ_BH]^-$. The changes at 420 nm following the second laser flash for RQ_B-RCs in the presence of the exogenous reductant ferrocene at three pH values are shown. The changes were well-fitted by a single exponential (solid lines) with characteristic times of ∼50, 150, and 260 μs at pH 6.5, 8.3, and 8.7, respectively. These decays were assigned to electron transfer. A faster transient (τ ∼ 3 μs), assigned to decay of the triplet state, was subtracted.

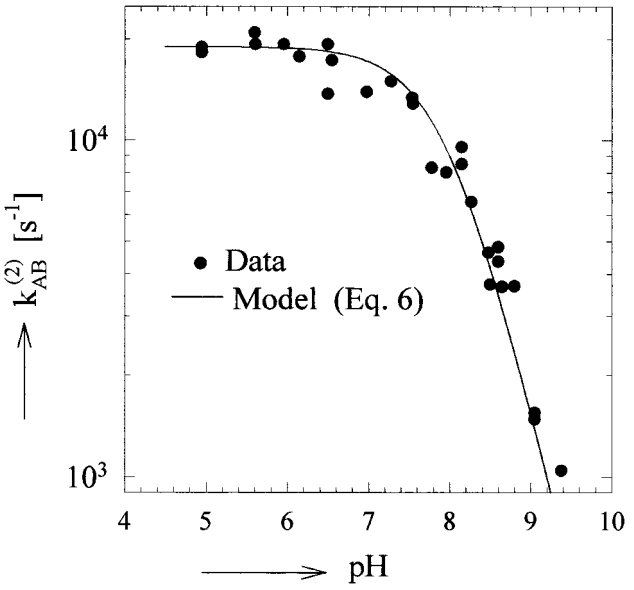

FIGURE 6: pH dependence of the second electron-transfer rate, $k_{AB}^{(2)}$, in RQ_B-RCs determined from the decay of semiquinone absorbance at 420 nm (Figure 5). The solid line represents the predicted dependence for the Proton-Activated Electron-Transfer mechanism $[Q_A^{-\bullet}Q_B^{-\bullet} + H^+ \rightleftharpoons Q_A^{-\bullet}(Q_BH)^\bullet \rightarrow Q_A(Q_BH)^-]$ (eq 6) with $pK_{RQ_BH^\bullet} = 8.0$. Conditions as in Figure 5.

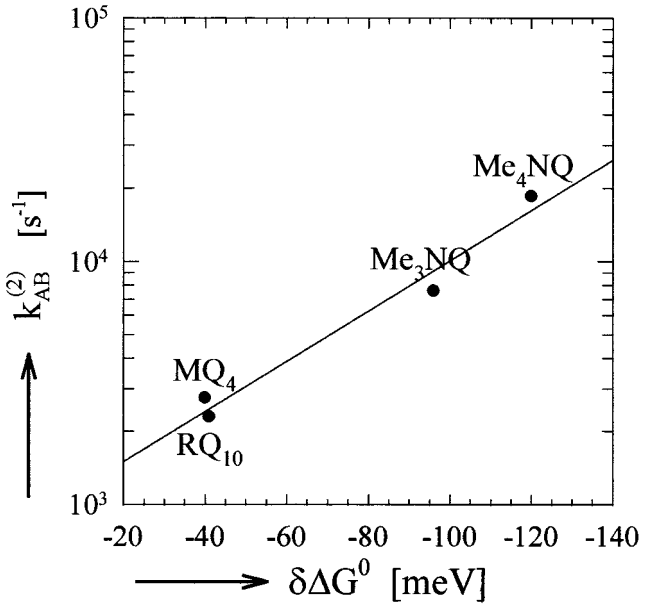

FIGURE 7: The second electron-transfer rate, $k_{AB}^{(2)}$, as a function of the change in redox free energy (driving force) for electron transfer. The quinones RQ, MQ_4, Me_3NQ, and Me_4NQ were substituted into the Q_A site. The Q_B site was occupied by RQ. The rate varied by a factor of 10 per 100 meV change in electron-transfer driving force showing that the reaction is rate limited by electron transfer. The line shows a smooth fit to the data. The statistical uncertainty in the measured rates was ≤10%. Uncertainties in the free energy values, which are given relative to Q_{10} in the Q_A site, were less than 10 meV. Conditions: 4−6 μM RQ_B-RCs, pH 4.95, 30 μM ferrocene.

Driving Force Dependence of $k_{AB}^{(2)}$ in RQ_B-RCs. The dependence of $k_{AB}^{(2)}$ on the redox potential of Q_A, i.e. the electron transfer driving force, has been used previously to determine the rate-limiting step of the proton-coupled electron-transfer reaction in native RCs (*4*). In this work, we employed the same method to investigate the rate-limiting step in RQ_B-RCs. Native Q_{10} in the Q_A site was replaced with RQ, MQ_4, Me_3NQ, and with Me_4NQ, while RQ was retained in the Q_B site. The relative *in situ* redox potentials of the non-native quinones in the Q_A site were determined from measurements of k_{AD} and k_{BD} as described previously (*4*). The observed rate $k_{AB}^{(2)}$ increased by a factor of 10 per 100 meV change in redox free energy (see Figure 7). These observations show that, like for native RCs, electron transfer is rate-limiting in RQ_B-RCs.

SUMMARY AND DISCUSSION

In this work, we have verified the previously proposed mechanism of proton-activated electron transfer (PAET) $k_{AB}^{(2)}$ [$Q_A^{-\bullet}Q_B^{-\bullet} + H^+ \rightleftarrows Q_A^{-\bullet}(Q_BH)^\bullet \rightarrow Q_A(Q_BH)^-$] in isolated RCs from *Rb. sphaeroides* by detecting the intermediate protonated state, $Q_BH^\bullet$. In this mechanism, a fast-reversible proton transfer, to form $Q_BH^\bullet$ precedes the rate-limiting electron transfer. To observe the intermediate state, we substituted into the Q_B site RQ, which has a higher p*K* value than native Q_{10}. The p*K* value of $RQ_BH^\bullet$ in the RC was determined from the pH dependences of three independent observables: the semiquinone optical spectrum, the rate of charge recombination, k_{BD}, and the rate of the proton-coupled electron transfer, $k_{AB}^{(2)}$. The intrinsic rate of electron transfer, k_{ET}, was obtained from the observed rate $k_{AB}^{(2)}$ (see eq 6) at low pH, at which $Q_B^{-\bullet}$ is fully protonated. From its value, a limit for the proton-transfer rate was established. The results obtained on the RQ_B-RC system were extrapolated to the native Q_{10}−RC system. These points are discussed in more detail below.

Observation of the Intermediate State, $Q_BH^\bullet$; Determination of its pK. The distinct optical spectrum of protonated semiquinone ($QH^\bullet$) offers a direct way to detect the presence of the $Q_BH^\bullet$ state; at low pH the spectrum of rhodosemiquinone strongly resembled that of a protonated semiquinone (Figure 2) (*26*). The most straightforward method to determine the fraction of $Q_BH^\bullet$, $f(Q_BH^\bullet)$, is by spectral titration (see Figures 2 and 3). By fitting $f(RQ_BH^\bullet)$ with a classical titration curve (eq 3) a value of p$K = 7.3 \pm 0.2$ was obtained. From the pH dependence of the charge recombination rate k_{BD} a p$K = 7.0 \pm 0.1$ was determined (see Figure 4 and eqs 4 and 5), which is in good agreement with the optically determined value.

The pH dependence of the second electron-transfer kinetics, $k_{AB}^{(2)}$, indicated a p*K* of 8.0 ± 0.2 (see Figure 6 and eq 6). This value is shifted from the values obtained by the other two methods, which were one electron assays, in which Q_A remained neutral. In the $k_{AB}^{(2)}$ assay, Q_A is reduced to $Q_A^{-\bullet}$. We, therefore, attribute the shift of 0.8 pH units to an electrostatic interaction between $Q_A^{-\bullet}$ and $Q_B^{-\bullet}$. Using a simple point-charge electrostatic analysis (Coulomb's Law) and the known distance (center-to-center) between Q_A and Q_B of 17 Å (*39*), one can account for the observed shift with an average dielectric constant of ∼20 for the intervening matrix between $Q_A^{-\bullet}$ and $Q_B^{-\bullet}$.

The Proton-Activated Electron Transfer (PAET) Mechanism. The predictions of the PAET mechanism are that (*i*) $k_{AB}^{(2)}$ should be approximately pH independent for pH ≪ p*K* of the intermediate state and should decrease by a factor of ∼10 per pH unit for pH ≫ p*K*.[2] (*ii*) $k_{AB}^{(2)}$ should be rate limited by electron transfer and thus should depend on the driving force for electron transfer and (*iii*) the intermediate, $Q_BH^\bullet$, should be observable as the pH is decreased toward the p*K* value. These predictions are in good agreement with the experimental findings (Figures 2, 3, 4, 6, and 7), thus, verifying the proposed mechanism for RQ_B-RCs. It should also be noted that the presence of an intermediate state eliminates the concerted proton−electron transfer mechanism that had not been definitively excluded previously (*4*).

Intrinsic Rate Constants. Proteins of the mitochondrial and photosynthetic electron transport chains catalyze *observed* reactions on the millisecond time scale. Examples of these are cytochrome oxidase, the cytochrome bc1 complex, the NADH−quinone reductase and the photsynthetic reaction center (*1*). Several of the observed millisecond reactions are likely to involve an undetected intermediate state and have rates associated with the intrinsic steps that are orders of magnitude larger than the observed rate. An example of such a situation is given by the RC studied in this work; the intrinsic rates, k_{ET} and k_{H^+}, are orders of magnitude larger than the *observed* millisecond rate, $k_{AB}^{(2)}$, as discussed below.

Intrinsic Electron-Transfer Rates. The observed rate of the first electron transfer $k_{AB}^{(1)}$ [$Q_A^{-\bullet}Q_B \rightarrow Q_AQ_B^{-\bullet}$] is governed by conformational gating and, therefore, is not a measure of the intrinsic electron-transfer rate. In contrast to

the $k_{AB}^{(1)}$ reaction, the proton-coupled second electron-transfer reaction, $k_{AB}^{(2)}$, is rate limited by electron transfer (see Figure 7). The observed rate is equal to the intrinsic electron-transfer rate multiplied by the fraction of protonated intermediate (eq 6), a quantity that had not been previously determined. In this work, we have shown that at low pH, $RQ^{-\bullet}$ becomes protonated, i.e. $f(Q_BH^\bullet) = 1$. Thus, at low pH, the measured $k_{AB}^{(2)}$ represents the intrinsic electron-transfer rate, i.e. $k_{AB}^{(2)} = k_{ET}$ (see eq 6). Its value was determined at pH $\ll$ pK to be $k_{ET}^{RQ_B} \sim 2 \times 10^4$ s^{-1}, see Figure 6.

How does the intrinsic electron-transfer rate [$Q_A^{-\bullet}Q_BH^\bullet \rightarrow Q_AQ_BH^-$] compare with the rate of other electron-transfer reactions? An empirical relation between the maximum rate of electron transfer and the distance between redox cofactors has been used to compare rates of electron transfer in different proteins (*42*). To extrapolate from the measured rate to the maximum rate, at which $-\Delta G^\circ = \lambda$, we use the free energy for electron transfer $\Delta G^\circ = -20$ meV and assume a λ of $\sim$1 eV (*4*, *36*, *43*−*44*). From this analysis, k_{ET}^{MAX} in RQ_B-RCs is $\sim 3 \times 10^8$ s^{-1}. The above-mentioned empirical relation predicts for the edge-to-edge distance between Q_A and Q_B of 14.5 Å (39) a maximum rate $k_{ET}^{MAX} \cong 10^6$ s^{-1}. This is more than 2 orders of magnitude smaller than the value deduced from the experimental data. The likely reason for this discrepancy is that the empirical relation assumes an average intervening protein medium, i.e. a combination of sigma bonds, hydrogen bonds, and no bonds ("through space jumps"). However, the medium between Q_A and Q_B in the RC deviates from the average: Q_A and Q_B are connected through hydrogen bonds to an Fe^{2+}-histidine complex (*39*) without any through-space jumps. The theoretical "pathways" model, (*45*−*48*) and "density of packing" model (*49*), which make an attempt to account for the distinct media between electron donors and acceptors, are in better agreement with the experimentally determined value.

Intrinsic Proton-Transfer Rates. The PAET mechanism predicts that the proton-transfer rate is much larger than the intrinsic electron-transfer rate. At pH = pK $\sim$ 7.5, the forward and reverse proton transfers are equal, and the electron transfer at this pH was found to be 2×10^4 s^{-1} (see above). Thus, we can establish a lower limit for the proton-transfer rate of $k_{H^+} \gg 2 \times 10^4$ s^{-1}. We can extend this limit to $k_{H^+} \gg 10^5$ s^{-1} by considering the kinetic decay of semiquinone absorption (Figure 5a). If $k_{H^+} < 10^5$ s^{-1}, biexponential kinetics would have been detected near the pK. The limit of $k_{H^+} \gg 10^5$ s^{-1} is larger than simple theory predicts for proton transfer from bulk solution at pH 7.5, which is 10^3 s^{-1} (*50*). Consequently, we conclude that the fast rate of proton transfer must arise either by second order proton transfer from solution enhanced by electrostatic interactions or by first order proton transfer from an internal proton donor (*51*). This transfer can be facilitated by the internal hydrogen-bonded network of protonatable amino acids and water molecules which surround Q_B (*39*, *52*−*54*).

Extrapolation of the Results from RQ_B-RCs to Native Q_{10}-RCs. The observation of the intermediate $Q_BH^\bullet$ state, the driving force dependence of $k_{AB}^{(2)}$ and the pH dependence of $k_{AB}^{(2)}$ show that the PAET mechanism is operative in RQ_B-RCs. In native RCs, two of these three observations were made: the driving force dependence in native RCs is similar to that of RQ_B-RCs and the PAET mechanism can quantitatively explain the pH dependence of $k_{AB}^{(2)}$ in native Q_{10}-RCs.[3] However, in isolated Q_{10}-RCs, the intermediate state, $Q_BH^\bullet$, is not observed. On the basis of the results from the RQ_B-RC system, we calculated for Q_{10}-RCs at pH 7.5 that $f(Q_BH^\bullet) = 10^{-3}$, consistent with a p$K$ of 4.5 $\pm$ 0.5[4] (see Appendix). This low pK indicates a small population of $Q_BH^\bullet$ at pH 7.5 and explains the lack of its observation. The calculated pK of $Q_BH^\bullet$ in the polar Q_B binding site is close to that estimated for $Q_{10}H^\bullet$ in aqueous solution (*56*). Interestingly, in chromatophores (RCs in their native environment), Lavergne et al. (*57*) reported pH dependent optical changes around pH 7. The authors interpreted these changes in terms of $Q_B^{-\bullet}$ protonation. If their interpretation is correct, the pK of $Q_BH^\bullet$ is increased by $\sim$3 units when the RCs are incorporated in the native membrane.

The intrinsic electron-transfer rate k_{ET} between $Q_A^{-\bullet}$ and $Q_BH^\bullet$ in Q_{10}-RCs was obtained by extrapolating the results from RQ-RCs using the Marcus theory of electron transfer (*41*) (see Appendix). Assuming that the values of the reorganization energy and the electronic matrix element are the same for both systems,[5] the rate of the intrinsic electron transfer at pH 7.5 is predicted to be $\sim 10^{6.0\pm0.2}$ s^{-1} (see Appendix).

To determine the values for the rate of proton transfer in native Q_{10}-RCs, we make use of the estimate for $f(Q_BH^\bullet)$ and the measured value for $k_{AB}^{(2)}$. For the first step, which involves the equilibration of the initial state $Q_A^{-\bullet}Q_B^{-\bullet}$ with the intermediate state $Q_A^{-\bullet}Q_BH^\bullet$, there are two intrinsic rate constants to consider − the rate of protonation of $Q_B^{-\bullet}$, k_H, and the rate of deprotonation of $Q_BH^\bullet$, k_{-H} (Figure 8). The equilibrium fraction of the intermediate state is given by $f(Q_BH^\bullet) = k_H/k_{-H} = 10^{-3}$. Since the reaction rate is limited

[3] We could describe the pH dependence of $k_{AB}^{(2)}$ in Q_{10}-RCs over the measured pH range from 5.5 to 10.5 with no arbitrary parameters from the rates and energies calculated from RQ_B-RC data (see Appendix), and by using a mean-field approximation (*34*) to model the pH dependent electrostatic interaction between $Q_B^{-\bullet}$ and titrating amino acid sites. The mean-field model accounts for electrostatic interactions using the measured proton uptake in native RCs (*29*−*33*), which is directly related to the thermodynamically averaged electrostatic interaction energy.

[4] In reality, at pH 4.5 $Q_B^{-\bullet}$ is not $^1/_2$ protonated as would be expected for a classically titrating site.[2] Because $Q_B^{-\bullet}$ interacts electrostatically with titrating amino acids, one calculates that $f(Q_BH)^\bullet \leq 0.08$ at pH 4.5 consistent with experiments in which $(Q_BH)^\bullet$ is not detected spectroscopically even at low pH (*4*).

[5] The assumption of constant λ and T_{AB} can be justified in several ways. The first is based on the nearly identical structures of the substituted quinone compared to native Q_{10}. This argument has been presented previously (*4*). Second, the kinetics of the $k_{AB}^{(1)}$ reaction are the same with Q_{10} as with RQ in the Q_B site. Since the $k_{AB}^{(1)}$ reaction is rate limited by protein dynamics that involve Q_B, this results indicates that substitution of RQ_B does not affect the dynamics of Q_B motion and supports the assumption that RQ interacts with the RC in a manner similar to native Q_{10}. Third, EPR data indicates that the rhodosemiquinone interacts magnetically with the non-heme iron approximately to the same extent as does ubisemiquionone. Thus, to first order, the distance between the iron atom and Q_B is unchanged which implies that the distance between Q_A and Q_B is also unchanged. Since T_{AB} is a function of distance, this result suggests that T_{AB} is not greatly affected in RQ_B-RCs.

[6] The energy difference between the two-electron states, $(NQ_A^{-\bullet})(RQ_B^{-\bullet}(H))$ and $(NQ_A)(RQ_BH)^-$, is assumed to be the same as that measured between the one-electron states, $(NQ_A^{-\bullet})(RQ_B)$ and $(NQ_A)(RQ_B^{-\bullet}(H))$, i.e. −20 meV at pH 7.5. The error in the assumed value is estimated as $\pm$ 25 meV.

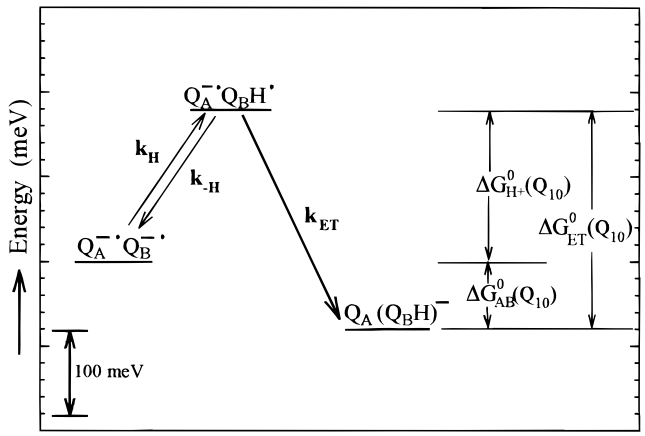

FIGURE 8: The states involved in the proton-coupled electron-transfer reaction, $k_{AB}^{(2)}$ for native Q_{10}-RCs at pH 7.5. The energies were calculated from the data obtained using RQ_B-RCs by correcting for the change in redox potential between Q_{10} and RQ (see Appendix). k_H and k_{-H} are the rates of protonation and deprotonation of the semiquinone, respectively, $k_{ET}^{Q_{10}}$ is the intrinsic electron-transfer rate ($10^{6.0\pm0.2}$ s^{-1}), $\Delta G_{H^+}{}^0(Q_{10})$ is the free energy to protonate $Q_B^{-\bullet}$(180 meV), $\Delta G_{AB}{}^0(Q_{10})$ is the free energy between initial and final states (−70 meV), and $\Delta G_{ET}{}^0(Q_{10})$ is the free energy for electron transfer (−250 meV).

by electron transfer, $k_H \gg k_{AB}^{(2)} = 10^3$ s^{-1}. The solution to these two equations yields $k_H \geq 10^4$ s^{-1} and $k_{-H} \geq 10^7$ s^{-1}.

The difference in the intrinsic rates of electron and proton transfer and the p*K* derived for Q_{10}-RCs from the RQ_B-RC results arise from the difference in the energy level of the intermediate state. However, the similarity of driving force and pH dependencies observed in Q_{10}-RCs (*4*, *21*) to those for the RQ_B-RCs show that the PAET mechanism is also operative in native Q_{10}-RCs.

ACKNOWLEDGMENT

We thank J. M. Bruce for Me_3NQ, Me_4NQ, and helpful discussions, J.M. Wright for assistance in obtaining NMR spectra of rhodoquinone and isorhodoquinone, and E.C Abresch and R.A. Isaacson for their expert technical assistance.

APPENDIX

Calculation of the pK_a of $Q_BH^\bullet$ and the Intrinsic Rate for the Second Electron Transfer in Native Q_{10}-RCs using RQ_B-RC Data. The states involved in the $k_{AB}^{(2)}$ reaction are shown in Figure 8. For RQ_B-RCs at pH 7.5, the initial state, $Q_A^{-\bullet}Q_B^{-\bullet}$, is approximately iso-energetic with the intermediate $Q_AQ_BH^\bullet$ state and the final state, $Q_A(Q_BH)^-$, is ∼20 meV below the energy of the intermediate. The observed rate is $\sim10^4$ s^{-1} (see Figure 6). For Q_{10}-RCs the observed rate is slower ($\sim10^3$ s^{-1}), even though the energy gap between the initial and final states is not very different for the two systems: the free energy gap for RQ_B-RCs, $\Delta G_{AB}{}^0(RQ)$, is −20 meV, while that for Q_{10}-RCs, $\Delta G^0{}_{AB}(Q_{10})$, is −70 meV (55), as shown in Figure 8. We propose that the difference in the observed rates is due to the energy difference between the intermediate states of the two systems. Qualitatively, if the energy of the intermediate state is raised, the observed rate is slowed due to the reduction of the intermediate state population. A faster electron transfer due to the increased electron transfer driving force, only partially compensates for this reduction in the $Q_BH^\bullet$ population. Thus, the effect of raising the energy of the intermediate state is a reduction in the observed rate. The increase in energy required to account for the difference in the observed rate between RQ_B-RCs and Q_{10}-RCs is calculated below.

The observed rate will be reduced because of the reduction in the Boltzmann population of the $Q_BH^\bullet$ intermediate by a factor:

$$\frac{f(Q_{10(B)}H^\bullet)}{f(RQ_{(B)}H^\bullet)} = \frac{(1+\exp[\Delta G^0_{H^+}(Q_{10})/k_BT])^{-1}}{(1+\exp[\Delta G^0_{H^+}(RQ)/k_BT])^{-1}} \quad \text{(A1)}$$

To calculate the increase in electron-transfer rate due to the increase in electron-transfer driving force in Q_{10}-RCs, we use the Marcus relation (41):

$$k_{ET} = \frac{2\pi|T_{AB}|^2}{\hbar\sqrt{4\pi\lambda k_BT}}\exp-\left[\frac{(\Delta G^0_{ET}+\lambda)^2}{4\lambda k_BT}\right] \quad \text{(A2)}$$

where k_{ET} is the intrinsic electron-transfer rate constant, $\Delta G^0{}_{ET}$ is the free energy for electron transfer (defined as the energy of the final minus the initial state), λ is the reorganization energy and T_{AB} is the tunneling matrix element. The observed rate will be increased by a factor $k_{ET}^{Q10}/k_{ET}^{RQ_B}$. Assuming that the substitution of RQ for Q_{10} does not significantly affect λ or T_{AB},[5] we obtain from eq A2:

$$\frac{k_{ET}^{Q10}}{k_{ET}^{RQ}} = \frac{\exp-\left[\frac{(\Delta G^0_{ET}(Q_{10})+\lambda)^2}{4\lambda k_BT}\right]}{\exp-\left[\frac{(\Delta G^0_{ET}(RQ)+\lambda)^2}{4\lambda k_BT}\right]} \quad \text{(A3)}$$

Referring to Figure 8, we define

$$\delta\Delta G^0 = \Delta G^0{}_{ET}(Q_{10}) - \Delta G^0{}_{ET}(RQ) \quad \text{(A4)}$$

where

$$\Delta G^0{}_{ET}(Q_{10}) = \Delta G^0{}_{AB}(Q_{10}) - \Delta G^0{}_{H^+}(Q_{10}) \quad \text{(A5)}$$

Expanding the exponentials in A3 and neglecting terms in $(\delta\Delta G^\circ)^2$, we obtain for the relative increase due to the change in electron-transfer driving force:

$$\frac{k_{ET}^{Q10}}{k_{ET}^{RQ}} = \exp-\left[\frac{\delta\Delta G^0}{2k_BT}\left(1+\frac{\Delta G^0_{ET}(Q_{10})}{\lambda}\right)\right] \quad \text{(A6)}$$

Combining eq A1 and A6 the relative change in the *observed* rate is given by:

$$\frac{k_{AB}^{(2)}(Q_{10})}{k_{AB}^{(2)}(RQ)} = \frac{(1+\exp[\Delta G^0_{H^+}(Q_{10})/k_BT])^{-1}}{(1+\exp[\Delta G^0_{H^+}(RQ)/k_BT])^{-1}} \times \exp-\left[\frac{\delta\Delta G^0}{2k_BT}\left(1+\frac{\Delta G^0_{ET}(Q_{10})}{\lambda}\right)\right] \quad \text{(A7)}$$

Equation A7 was solved for $\Delta G^0_{H^+}(Q_{10})$ by expanding the exponentials. and using the following measured values (pH 7.5)

parameter	value	reference
$k_{AB}^{(2)}$ (RQ)	$2 \times 10^4\ s^{-1}$	this work
$k_{AB}^{(2)}$ (Q_{10})	$1.4 \times 10^3\ s^{-1}$	(*30*)
$\Delta G_{H^+}^0$(RQ)	0 ± 10 meV	this work
ΔG_{AB}^0 (Q_{10})	-70 ± 10 meV	(*55*)
ΔG_{ET}^0(RQ)	-20 ± 25 meV	this work

For $\lambda = 1.2$ eV (*36*), $\Delta G_{H^+}^0(Q_{10})$ was determined to be 180 $\pm$ 30 meV, corresponding to a p$K \sim 4.5 \pm 0.5$. This value was substituted into eq A6 to obtain the value for $k_{ET}^{Q_{10}} = 10^{6.0\pm0.2}\ s^{-1}$.

REFERENCES

1. Cramer, W. A., and Knaff, D. B. (1990) *Energy Transduction in Biological Membranes*, Springer-Verlag, New York.
2. Blankenship, R. E., Madigan, M. T., and Bauer, C. E. (1995) *Anoxygenic Photosynthetic Bacteria*, Kluwer Academic Publishers, Dordrecht.
3. Okamura, M. Y., and Feher, G. (1995) in *Anoxygenic Photosynthetic Bacteria* (Blankenship, R. E., Madigan, M. T., and Bauer, C. E., Eds.) Vol. 2, pp 577−594, Kluwer Academic Publishers, Dordrecht.
4. Graige, M. S., Paddock, M. L., Bruce, J. M., Feher, G., and Okamura, M. Y. (1996) *J. Am. Chem. Soc. 118*, 9005−9016.
5. Cukier, R. I. (1994) *J. Phys. Chem. 98*, 2377−2381.
6. Fang, J. Y., and Hammes-Schiffer, S. (1997) *J. Chem. Phys. 106*, 8442−8454.
7. Cukier, R. I., and Nocera, D. G. (1998) *Annu. Rev. Phys. Chem. 49*, 337−369.
8. Erabi, T., Higuti, T., Kakuno, T., Yamashita, J., Tanaka, M., and Horio, T. (1975) *J. Biochem. (Tokyo) 78*, 795−801.
9. Graige, M. S., Paddock, M. L., Feher, G., and Okamura, M. Y. (1997) *Biophys. J. 72*, A7.
10. Sistrom, W. R. (1977) *J. Bacteriol. 131*, 526−532.
11. Grover, J., and Threlfall, D. R. (1962) *Biochem. J. 85*, 14P.
12. Redfearn, E. R. (1967) *Biochim. Biophys. Acta 131*, 218−220.
13. Moore, H. W., and Folkers, K. (1966) *J. Am. Chem. Soc. 88*, 567−570.
14. Daves, G. D., Wilczynski, J. J., Friis, P., and Folkers, K. (1968) *J. Am. Chem. Soc. 90*, 5587−5593.
15. Paddock, M. L., Rongey, S. H., Abresch, E. C., Feher, G., and Okamura, M. Y. (1988) *Photosynth. Res. 17*, 75−96.
16. Okamura, M. Y., Isaacson, R. A., and Feher, G. (1975) *Proc. Natl. Acad. Sci. U.S.A. 72*, 3491−3495.
17. Woodbury, N. W., Parson, W. W., Gunner, M. R., Prince, R. C., and Dutton, P. L. (1986) *Biochim. Biophys. Acta 851*, 6−22.
18. Okamura, M. Y., Debus, R. J., Kleinfeld, D., and Feher, G. (1982) in *Functions of Quinones in Energy Conserving Systems* (Trumpower, B. L., Ed.) Academic Press, New York, pp 299−317.
19. Kleinfeld, D., Okamura, M. Y., and Feher, G. (1984) *Biochim. Biophys. Acta 766*, 126−740.
20. Graige, M. S., Feher, G., and Okamura, M. Y. (1998) *Proc. Nat. Acad. Sci. 95*, 11679−11684.
21. Kleinfeld, D., Okamura, M. Y., and Feher, G. (1985) *Biochim. Biophys. Acta 809*, 291−310.
22. Stein, R. R., Castellvi, A. L., Bogacz, J. P., and Wraight, C. A. (1984) in *Biosynthesis of the Photosynthetic Apparatus: Molecular Development, and Regulation* (Hallick, R., L. A. S., Thornber, J. P., Ed.), pp 167−183, Alan R. Liss, New York.
23. Okamura, M. Y. (1984) in *Biosynthesis of the Photosynthetic Apparatus: Molecular Development and Regulation* (Hallick, R., L. A. S., Thornber, J. P., Eds.), Alan R. Liss, New York, pp 381−390.
24. Vermeglio, A. (1977) *Biochim. Biophys. Acta 459*, 516−524.
25. Wraight, C. A. (1979) *Biochim. Biophys. Acta 548*, 309−327.
26. Land, E. J., Simic, M., and Swallow, A. J. (1971) *Biochim. Biophys. Acta 226*, 239−240.
27. Tanford, C., and Kirkwood, J. G. (1957) *J. Am. Chem. Soc. 79*, 5333−5339.
28. Edsall, J. T., and Wyman, J. (1958) *Biophysical Chemistry*, Acad. Press, NewYork.
29. McPherson, P. H., Okamura, M. Y., and Feher, G. (1988) *Biochim. Biophys. Acta 934*, 348−368.
30. McPherson, P. H., Okamura, M. Y., and Feher, G. (1993) *Biochim. Biophy. Acta 1144*, 309−324.
31. Maroti, P., and Wraight, C. A. (1988) *Biochim. Biophys. Acta 934*, 314−328.
32. Maroti, P., and Wraight, C. A. (1988) *Biochim. Biophys. Acta 934*, 329−347.
33. Kalman, L., and Maroti, P. (1994) *Biochemistry 33*, 9237−9244.
34. Tanford, C., and Roxby, R. (1972) *Biochemistry 11*, 2192−2198.
35. Gunner, M. R., Tiede, D. M., Prince, R. C., and Dutton, P. L. (1982) in *Functions of Quinones in Energy Conserving Systems* (Trumpower, B. L., Ed.) Academic Press, New York, pp 265−269.
36. Labahn, A., Bruce, J. M., Okamura, M. Y., and Feher, G. (1995) *Chemical Physics 197*, 355−366.
37. Brzezinski, P., Okamura, M. Y., and Feher, G. (1992) in *The Photosynthetic Bacterial Reaction Center II: Structure, Spectroscopy and Dynamics* (Breton, J., and Vermeglio, A., Eds.), Plenum Press, New York, pp 321−330.
38. Li, J. L., Gilroy, D., Tiede, D. M., and Gunner, M. R. (1998) *Biochemistry 37*, 2818−2829.
39. Stowell, M. H. B., McPhillips, T. M., Rees, D. C., Soltis, S. M., Abresch, E., and Feher, G. (1997) *Science 276*, 812−816.
40. Monger, T. G., Cogdell, R. J., and Parson, W. W. (1976) *Biochim. Biophys. Acta 449*, 136−153.
41. Marcus, R. A., and Sutin, N. (1985) *Biochim. Biophys. Acta 811*, 265−322.
42. Moser, C. C., Keske, J. M., Warncke, K., Farid, R. S., and Dutton, P. L. (1992) *Nature 355*, 796−802.
43. Labahn, A., Paddock, M. L., McPherson, P. H., Okamura, M. Y., and Feher, G. (1994) *J. Phys. Chem. 98*, 3417−3423.
44. Allen, J. P., Williams, J. C., Graige, M. S., Paddock, M. L., Labahn, A., Feher, G., and Okamura, M. Y. (1998) *Photosynth. Res. 55*, 227−233.
45. Beratan, D. N., Betts, J. N., and Onuchic, J. N. (1991) *Science 252*, 1285−1288.
46. Beratan, D. N., Onuchic, J. N., Winkler, J. R., and Gray, H. B. (1992) *Science 258*, 1740−1741.
47. Curry, W. B., Grabe, M. D., Kurnikov, I. V., Skourtis, S. S., Beratan, D. N., Regan, J. J., Aquino, A. J. A., Beroza, P., and Onuchic, J. N. (1995) *J. Bioenerget. Biomem. 27*, 285−293.
48. Farver, O., and Pecht, I. (1997) *J. Biol. Inorg. Chem. 2*, 387−392.
49. Moser, C. C., Page, C. C., Chen, X., and Dutton, P. L. (1997) *J. Biol. Inorg. Chem. 2*, 393−398.
50. Bell, R. P. (1959) *The Proton in Chemistry*, Cornell University Press, Ithaca.
51. Paddock, M. L., Graige, M. S., Feher, G., and Okamura, M. Y. (1999) *Proc. Natl. Acad. Sci USA 96*, 6183−6188.
52. Ermler, U., Fritzsch, G., Buchanan, S. K., and Michel, H. (1994) *Structure 2*, 925−936.
53. Abresch, E. C., Paddock, M. L., Stowell, M. H. B., McPhillips, T. M., Axelrod, H. L., Soltis, S. M., Rees, D. C., Okamura, M. Y., and Feher, G. (1998) *Photosynth. Res. 55*, 119−125.
54. Fritzsch, G., Kampmann, L., Kapaun, G., and Michel, H. (1998) in *Photosynthesis: Mechanisms and Effects, Vol II*, (Garab, G., Ed.), pp 861−864 (Kluwer Academic Publishers, Netherlands).
55. McPherson, P. H., Schonfeld, M., Paddock, M. L., Okamura, M. Y., and Feher, G. (1994) *Biochemistry 33*, 1181−1193.
56. Swallow, A. J. (1982) in *Functions of Quinones in Energy Conserving Systems* (Trumpower, B. L., Ed.) Academic Press, New York, pp 59−72.
57. Lavergne, J., Matthews, C., and Ginet, N. (1999) *Biochemistry 38*, 4542−4552.

BI990708U